High-accuracy Rb_2^+ interaction potentials based on coupled-cluster calculations

Jan Schnabel [1,*] Lan Cheng [2,†] and Andreas Köhn [1,‡]

[1]*Institute for Theoretical Chemistry and Center for Integrated Quantum Science and Technology, University of Stuttgart, 70569 Stuttgart, Germany*

[2]*Department of Chemistry, The Johns Hopkins University, Baltimore, Maryland 21218, USA*

(Received 22 June 2022; accepted 23 August 2022; published 8 September 2022)

This work discusses a protocol for constructing highly accurate potential energy curves (PECs) for the lowest two states of Rb_2^+, i.e., $X\,^2\Sigma_g^+$ and $(1)\,^2\Sigma_u^+$, using an additivity scheme based on coupled-cluster theory. The approach exploits the findings of our previous work [J. Schnabel, L. Cheng, and A. Köhn, J. Chem. Phys. **155**, 124101 (2021)] to avoid the unphysical repulsive long-range barrier occurring for symmetric molecular ions when perturbative estimates of higher-order cluster operators are employed. Furthermore, care was taken to reproduce the physically correct exchange splitting of the $X\,^2\Sigma_g^+$ and $(1)\,^2\Sigma_u^+$ PECs. The accuracy of our computational approach is benchmarked for ionization energies of Rb and for spectroscopic constants as well as vibrational levels of the $a\,^3\Sigma_u^+$ triplet state of Rb_2 . We study high-level correlation contributions, high-level relativistic effects, and inner-shell correlation contributions and find very good agreement with experimental reference values for the atomic ionization potential and the binding energy of Rb_2 in the $a\,^3\Sigma_u^+$ triplet state. Our final best estimate for the binding energy of the Rb_2^+ $X\,^2\Sigma_g^+$ state including zero-point vibrational contributions is $D_0 = 6179\ \mathrm{cm}^{-1}$ with an estimated error bound of $O(\pm 30\ \mathrm{cm}^{-1})$. This value is smaller than the experimentally inferred lower bond of $D_0 \geqslant 6307.5\ \mathrm{cm}^{-1}$ [M. A. Bellos *et al.*, Phys. Rev. A **87**, 012508 (2013)] and will require further investigation. For the $(1)\,^2\Sigma_u^+$ state a shallow potential with $D_0 = 78.4\ \mathrm{cm}^{-1}$ and an error bound of $\pm 9\ \mathrm{cm}^{-1}$ is computed.

DOI: 10.1103/PhysRevA.106.032804

I. INTRODUCTION

The recent experimental progress [1–6] towards entering the ultracold ($T < 1$ mK) quantum regime of hybrid ion-atom systems is naturally entangled with the need for accurate theoretical models based on first principles. While the cold regime ($T > 1$ mK) of ion-atom collisions is essentially classical, the ultracold domain allows for s-wave collisions and thus for reaching the pure quantum regime. The realization is still a nontrivial task for hybrid ion-atom systems due to more stringent temperature requirements, in particular for Rb_2^+ [7]. Ultracold ion-atom systems provide a rich platform allowing for the discovery of novel phenomena and applications [2]. Among others, those may reach from precision measurements of ion-atom collision parameters and associated molecular potentials [1,8,9] to ultracold state-resolved quantum chemistry [10] and to the ultimate goal of realizing strongly coupled charge-neutral polaron systems [11–13]. For a comprehensive overview on both the theoretical and experimental state-of-the-art research on cold hybrid ion-atom systems see, e.g., Refs. [7,14].

The successful experimental realization of an ultracold ion-atom system has been demonstrated in Ref. [1] for Li_2^+. The idea of this class of experiments starts with implanting an ionic impurity into a Bose-Einstein condensate through a single precursor Rydberg atom followed by subsequent ionization to initiate collisions with the ionic core and the ground-state host gas atoms.

For Rb_2^+, initial experiments date back to the 1960s to 1980s and have been performed in Rb vapor with densities of 2.69×10^{19} atoms cm^{-3} [15]. Corresponding measurements range from associative photoionization [15,16] to rough estimates based on the analysis of charge-exchange cross sections [17] to multiphoton ionization of Rb_2 and subsequent dissociation of dimer ions by one or more additional photons [18]. More recent experiments [1–6] used the same technique as described for Li_2^+. In this way, the diffuse transport dynamics of the impurity through the BEC and ion-atom-atom three-body recombination could be observed [4,5,19]. In Ref. [4] it was even possible to estimate the binding energies of some threshold bound states. These experiments may thus offer a way to probe chemical reaction channels at the quantum level. This so-called state-to-state chemistry will require resolving the quantized molecular energy levels both theoretically and experimentally.

Recent theoretical investigations of X_2^+ systems (with X = Li, Na, K, Rb) can be found, e.g., in Refs. [20–27]. The equation-of-motion coupled-cluster method for electron-attached states with single and double replacements (EA-EOM-CCSD) or even including triple replacements (EA-EOM-CCSDT) and including scalar-relativistic effects via the Douglas-Kroll-Hess method has been used for calculations of Li_2^+, Na_2^+, and K_2^+ [25–27]. The authors reported satisfactory

*schnabel@theochem.uni-stuttgart.de
†lcheng24@jhu.edu
‡koehn@theochem.uni-stuttgart.de

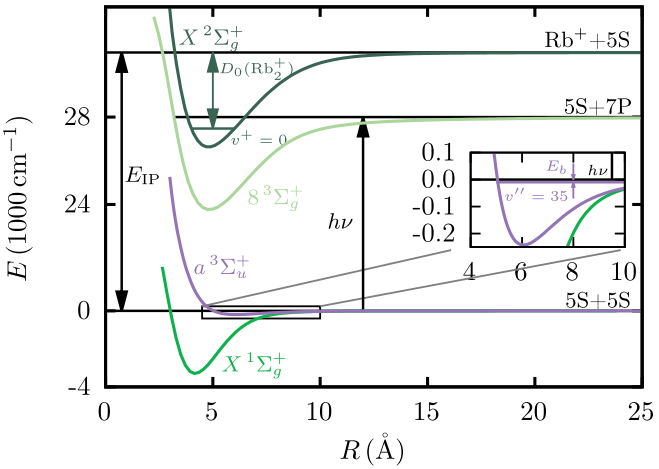

FIG. 1. Schematic overview on relevant potential energy curves of Rb_2 and Rb_2^+ to obtain a lower bound for $D_0(Rb_2^+)$ based on the experimental approach reported in Ref. [33]. This requires the atomic Rb ionization energy E_{IP}, the binding energy E_b (see inset) of the $v'' = 35$ vibrational level of the $a\,^3\Sigma_u^+$ state of Rb_2 (initial state for photoexcitation), as well as the photon energy $h\nu$ required for the onset of autoionization (via a "superexcited" level of the $8\,^3\Sigma_g^+$ state of Rb_2). (Inspired by a figure of M. A. Bellos *et al.* [33]).

agreement with available experimental results. As perhaps the only work aiming at highest possible accuracy, Schmid *et al.* [1] reported *ab initio* calculations for the Li_2^+ interaction potential based on an additivity scheme with coupled-cluster (CC) computations and large basis sets. These findings accompany the respective experimental work in Ref. [1], which were for the first time precise enough to predict reasonable bounds for the $Li+Li^+$ scattering length.

With this work we attempt to provide a general route for obtaining high-accuracy interaction potentials for the alkaline X_2^+ systems based on an additivity scheme using CC theory. The approach is inspired by the HEAT(high accuracy extrapolated *ab initio* thermochemistry) protocol [28–30], which allows for computing binding energies with uncertainties on the order of $\lhd 1$ kJ/mol, which translates into $\lhd 84$ cm^{-1}. By including our latest findings [31,32] to circumvent the wrong asymptotic behavior of some of the CC approximations required in this scheme, we report Rb_2^+ potential energy curves (PECs) with so far unprecedented precision. The binding energy derived from the computed $X\,^2\Sigma_g^+$ potential can be compared to the experimentally derived [33] lower bound for D_0^{expt}. This experiment aimed at measuring an upper bound to the ionization energy of $^{85}Rb_2$ formed via photoassociation, which also provides a lower bound to the dissociation energy of Rb_2^+. The bounds were measured by the onset of autoionization of the excited states of $^{85}Rb_2$ below the 5S+7P atomic limit. As illustrated in Fig. 1, D_0^{expt} of Rb_2^+ can be derived given the atomic ionization potential E_{IP}, the binding energy $E_b[Rb_2(v'' = 35)]$ of the initial state, and the applied photon energy $h\nu$, which causes the onset of autoionization.

Aside from computing spectroscopic constants, we provide analytical representations of our precise *ab initio* potentials, which may serve as foundation to facilitate more sophisticated scattering calculations for more quantitative statements on the conditions needed to identify effects for $Rb+Rb^+$ collisions that go beyond the Langevin regime. Conventional approaches [10,19,34] for studying these collision processes are merely based on model potentials.

This paper is organized as follows. Section II introduces several computational aspects of this work, including the additivity scheme proposed to potentially reach high accuracy. We gauge the expected accuracy and limitations of our approach in Sec. III in terms of benchmark calculations for ionization energies of Rb and spectroscopic constants as well as vibrational levels of the $a\,^3\Sigma_u^+$ triplet ground state of Rb_2. Hereafter we investigate the prospects for obtaining highly accurate ground-state PECs of the Rb_2^+ system in Sec. IV. Therefore, we provide a protocol for constructing physically meaningful interaction potentials based on CC calculations. By thoroughly investigating basis-set effects and high-level correlation contributions, we infer reasonable error bars of our computational approach and demonstrate that the latter are less important to closely reproduce experimental findings. We provide spectroscopic constants and explore the rovibrational structure of the $X\,^2\Sigma_g^+$ and $(1)\,^2\Sigma_u^+$ states of Rb_2^+. Finally, we summarize the main findings of this work in Sec. V.

II. COMPUTATIONAL ASPECTS

High-accuracy quantum-chemical calculations of atomic and molecular energies often rely on additivity schemes [28,35–39]. Our approach follows the HEAT protocol [28–30], where we assume that the total electronic energy E can be calculated via

$$E = E_{\text{HF}}^{\infty} + \Delta E_{\text{CCSD(T)}}^{\infty} + \Delta E_{\text{HLC}} + \Delta E_{\text{HLR}}. \tag{1}$$

Herein, E_{HF}^{∞} and $\Delta E_{\text{CCSD(T)}}^{\infty}$ are the Hartree-Fock energy and the CCSD(T) correlation energy, respectively, at the complete basis set (CBS) limit. Correlation effects beyond CCSD(T) are denoted as high-level correlation (HLC) contributions ΔE_{HLC} and high-level relativistic (HLR) effects are labeled by ΔE_{HLR}.

The Hartree-Fock and coupled-cluster calculations are performed using either the small-core effective core potential (scECP) ECP28MDF from Ref. [40], where only the $4s^2 4p^6 5s^1$ electrons of Rb are treated explicitly and all the others are modeled via a scalar-relativistic pseudopotential (PP) or using the all-electron spin-free exact two-component theory in its one-electron variant (SFX2C-1e) [41,42] to treat scalar-relativistic effects. We use the restricted open-shell (ROHF) approach for the Hartree-Fock part and for generating the orbitals for the subsequent single-reference CC calculations. For the latter, we applied an unrestricted spin-orbital formalism in its singles and doubles variant augmented with a noniterative triples method based on a ROHF reference, the ROHF-UCCSD(T) method [43–46].

The HLC contributions considered in this work include the full triples correction obtained as the difference between full CC singles, doubles, and triples (CCSDT) [47–50] and CCSD(T) results using smaller basis sets (i.e., e.g., triple- and quadruple-ζ quality) and the quadruples correction obtained as the difference between CC singles, doubles, and triples augmented with noniterative quadruples [CCSDT(Q)] [51–53] and CCSDT results (at the triple-ζ level); cf. Sec. III. Here we

used the CCSDT(Q)/B variant for ROHF references [54]. The same convergence thresholds for the HF and CC calculations as described in our previous work on the Rb_2^+ system [31] were employed.

The aug-cc-pCVnZ-PP and aug-cc-pwCVnZ-PP ($n = 3, 4, 5$) correlation-consistent basis sets for alkali-metal and alkaline earth atoms, designed for the ECP28MDF pseudopotential [55], have been used. Furthermore, motivated by the promising results obtained in our recent work on Rb_3 [56], we constructed a large [17s14p9d7f6g5h4i] uncontracted even-tempered basis set (≡ UET17) based on the given valence basis set coming with the ECP28MDF pseudopotential in Ref. [40] (see Supplemental Material [57] for details). To obtain a better estimate on the Hartree-Fock limit, we combined an uncontracted and extended version of the aug-cc-pCV5Z-PP basis set for s, p, d, and f exponents with diffusely augmented g, h, and i functions of the UET17 basis; cf. Supplemental Material [57] for technical details and Table S.II for the respective exponents. We will call this basis "reference" in the following.

For the computations with the SFX2C-1e approach a different type of basis set is required. As the corresponding aug-cc-pwCVnZ-X2C basis sets are only available up to $n = 4$ [55], we used the s-, p- and d-type primitive functions of the uncontracted ANO-RCC (23s, 19p, 11d) set [58] and augmented them with f-, g-, h-, and i-type functions of our UET17 basis set, which were further complemented by four steeper functions to be able to describe core-valence correlation effects from the M shell (3s3p3d) (see Table S.III of the Supplemental Material [57]). These basis sets will be called UANO-n with $n = 3, 4, 5, 6$ in this work. To finally check basis-set saturation in the Hartree-Fock contribution, we replaced the s-, p-, and d-type functions by the decontracted basis functions from the aug-cc-pwCVQX-X2C basis and will call this basis "reference (ae)." The h- and i-type functions were skipped in this case to keep the size of the calculations at a manageable level. These higher-order angular momentum functions are not expected to contribute significantly at the Hartree-Fock level. See Table S.IV of the Supplemental Material [57].

In detail, we used the following protocol for evaluating the theoretical best estimates of the total energy according to Eq. (1): The Hartree-Fock CBS limit is obtained by a separate computation with the reference basis sets, as described above:

$$E_{\mathrm{HF}}^{\infty} \approx E_{\mathrm{HF}}(\text{reference basis}), \tag{2}$$

The correlation energy at the CBS limit is computed as

$$\Delta E_{\mathrm{CCSD(T)}}^{\infty} \approx E_{\mathrm{singles}}(n = n_{\mathrm{max}}) + E_{\mathrm{pair}}^{\infty} + E_{\mathrm{(T)}}^{\infty}. \tag{3}$$

Here, E_{singles} is the CCSD energy contribution resulting from the nonfulfillment of the Brillouin condition for the ROHF orbitals. We found it advantageous not to extrapolate this contribution along with the pair and triples energies as it has a distinctly different convergence behavior and saturates quickly with increasing cardinal number. Thus, we prefer to take the value for the highest available basis-set result ($n = 6$). The pair energy ($E_{\mathrm{pair}}^{\infty}$) and the noniterative triples ($E_{\mathrm{(T)}}^{\infty}$) contributions are extrapolated to their respective CBS limit using the conventional two-point n^{-3} formula [36,59]. The same procedure was followed for ECP and SFX2c-1e computations. In the latter case, we either correlated only the 4s4p and 5s shell (the electrons explicitly treated in the ECP approach) or we also included the 3s3p3d shell (M shell) into the correlation treatment to investigate further core-valence correlation effects. We note that other schemes for CBS extrapolation exist [60–63], but as demonstrated in Table S.V of the Supplemental Material [57] this has little impact on the accuracy of the extrapolated values.

The HLC contributions are computed via

$$\Delta E_{\mathrm{T}}^{\mathrm{TZ/QZ}} = E_{\mathrm{CCSDT}}^{\mathrm{TZ/QZ}} - E_{\mathrm{CCSD(T)}}^{\mathrm{TZ/QZ}}, \tag{4a}$$

$$\Delta E_{\mathrm{(Q)}}^{\mathrm{TZ}} = E_{\mathrm{CCSDT(Q)}}^{\mathrm{TZ}} - E_{\mathrm{CCSDT}}^{\mathrm{TZ}}, \tag{4b}$$

where we relied on ECP-based calculations and the aug-cc-pCVnZ-PP (n = T, Q) basis sets. As indicated by the superscript "TZ/QZ," the increment for the CCSDT contribution is obtained by extrapolating the correlation energies with the aug-cc-pCVTZ-PP and aug-cc-pCVQZ-PP basis sets using the two-point n^{-3} formula. The CCSDT(Q) computations used the aug-cc-pCVTZ-PP basis.

The considered high-level relativistic effects are relevant as corrections for the SFX2C-1e approach only. They consist of the two-electron picture-change (2e-pc) corrections, spin-orbit (SO) corrections, and the contributions from the Breit term. In addition, there are effects from quantum electrodynamics (QED) [64–66], which we did not attempt to compute here. The 2e-pc correction is obtained as the difference between the spin-free Dirac-Coulomb (SFDC) [67] and SFX2C-1e results. The SO correction together with the contribution from the Breit term is calculated as the difference between the spin-orbit X2C scheme with atomic mean-field spin-orbit integrals (X2CAMF) based on the Dirac-Coulomb-Breit Hamiltonian [68,69] and the SFX2C-1e scheme. Calculations of these contributions have been carried out at the CCSD(T) level using the uncontracted ANO-RCC basis set, employing the frozen-core approximation for the 1s2s2p3s3p3d shells and deleting virtual orbitals higher than 1000 E_{h}.

We note that it is less straightforward to incorporate ΔE_{HLR} into ECP calculations. This is due to the fact that the ECP28MDF pseudopotential already contains a two-component spin-orbit-coupled part with corresponding parameters adjusted to valence energies obtained at all-electron multiconfiguration Dirac-Coulomb–Hartree-Fock (DC-HF) level of theory, which includes relativistic effects at a four-component level of theory [40]. Therefore, one cannot use the difference between SFX2C-1e and high-level relativistic effects and ECP results as the correction to ECP. Furthermore, the quality of the basis sets used in the SFX2C-1e calculations is not exactly the same as those for the ECP calculations, so taking the difference introduces additional errors.

All ROHF-UCCSD(T) calculations have been performed with the MOLPRO 2019.2 program package [70–72], the CCSDT calculations have been carried out using the CFOUR program package [46,73–76], and all CCSDT(Q) energies were computed with the MRCC program suite [53,77–79].

TABLE I. Results for the Rb ionization energy E_{IP} (in cm^{-1}). The $4s4p$ and $5s$ shells are correlated unless noted otherwise. The experimental value is $E_{IP}^{expt} = 33\,690.81\ cm^{-1}$ [80,81].

	ECP		SFX2C-1e	
	apCVnZ-PP	UET17	UANO	UANO (M shell)[a]
$n = 4$	33550.89	33644.35	33561.48	33639.48
$n = 5$	33606.14	33664.46	33581.71	33660.87
$n = 6$		33671.71	33589.01	33668.26
CBS (corr)[b]	33665.87	33681.74	33599.11	33678.50
CBS (HF+corr)[c]		33675.96	33601.49	33680.89
$\Delta E_{T}^{TZ/QZ}$	2.40	[2.40]	[2.40]	[2.40]
$\Delta E_{(Q)}^{TZ}$	7.63	[7.63]	[7.63]	[7.63]
$\Delta E_{(Q)}^{TZ/QZ}$	10.72	[10.72]	[10.72]	[10.72]
$+\Delta E_{HLR}$			17.75	17.75
TBE[d]	33675.90	33685.99	33629.57	33708.96
TBE(ext)[e]	33678.99	33689.08	33632.66	33712.05

[a] *3s3p3d* shell included in correlation treatment.
[b] Extrapolation of correlation energy only, Hartree-Fock energy from largest n.
[c] Including a correction for Hartree-Fock limit using the "reference" basis sets.
[d] Theoretical best estimate (see text).
[e] Theoretical best estimate using $\Delta E_{(Q)}^{TZ/QZ}$ instead of $\Delta E_{(Q)}^{TZ}$.

III. BENCHMARK CALCULATIONS

In the following we benchmark the protocol described in Sec. II to assess both its expected accuracy and its limitations based on experimental reference values for Rb and Rb_2 .

A. Rb ionization potential

Calculations of the ionization potential (IP) of atomic Rb are listed in Table I. Comparison to the results using the aug-cc-pCVnZ-PP basis shows that the UET17 indeed leads to a much tighter convergence of the correlation energy. The gap between the $n = 6$ result and the estimated CBS limit of the IP is only $\sim$10 cm^{-1} and this observation also holds for the all-electron calculations with the UANO basis. We may therefore estimate the uncertainty of this result to be at most half of this difference. It is also evident from the two last columns of Table I that there is a significant contribution from the M-shell correlation of nearly 80 cm^{-1}. Interestingly, the ECP result (that only implicitly includes the effect of inner shells) is rather close to the SFX2C-1e result *with* explicit M-shell correlation (see line CBS in Table I). As the effect of core correlation will be much smaller in the other cases where we mainly look at binding energies, we did not go into further detail regarding this observation. Clearly, this points at the limits of the accuracy of the ECP approximation.

Moving to a larger basis for the Hartree-Fock contribution leads to corrections of the IP by 6 and 2 cm^{-1} for the ECP approach and the all-electron calculations, respectively. As a conservative estimate of the residual uncertainty for the Hartree-Fock contribution we thus take 5 cm^{-1}. The high-level correlation effects have been evaluated for the ECP/aug-cc-pCVnZ-PP computations only. The overall result is a contribution of 10 cm^{-1}. For the atoms, it was also feasible to carry out the CCSDT(Q) calculations with a quadruple-ζ quality basis set, which allowed a basis-set extrapolation for this quantity as well, leading to another 3 cm^{-1}. Overall, the contribution of ΔE_{HLC} is not very large and we will in the following use its total value as an estimate of the overall uncertainty in the correlation energy due to higher-order correlation (for the case of the IP of Rb: 10 cm^{-1}).

Finally, we consider the high-level relativistic (HLR) corrections beyond SFX2C-1e, ΔE_{HLR}. The two-electron picture change correction gives 5.76 cm^{-1} and the inclusion of spin-orbit coupling and the Breit term contributes 2.01 cm^{-1} further. In addition, a QED correction of 9.98 cm^{-1} has been taken from Ref. [66]. These three contributions add up to $\Delta E_{HLR} = 17.75\ cm^{-1}$ as given in Table I. The uncertainty in this correction may be conservatively estimated as roughly half its amount (10 cm^{-1}); we will later find much smaller relativistic corrections in the calculation of binding energies, which will then allow us to gauge the uncertainty by the total size of the high-level relativistic correction.

The final best estimates may be compared to the experimental value of $E_{IP}^{expt} = 33\,690.81 \pm 0.01\ cm^{-1}$ [80,81]. We find a deceptively good coincidence of the ECP-based result, in particular, if the extrapolated CCSDT(Q) results are taken into account. However, the error estimates discussed so far add up to approximately $\pm$30 cm^{-1}. Using this error bound, the overall X2C-based theoretical best estimate of 33 709 cm^{-1} is also in good agreement with the experimental value. The core-correlation from the M shell seems to be important for quantitative predictions and will be closely analyzed for its impact on the binding energies. It is most likely dominated by the $3d$ subshell, which is energetically significantly higher than the $3s$ and $3p$ subshells. The correlation from lower-lying shells (K and L) is much less important, as exploratory computations show (although with not fully sufficient basis sets, as even steeper polarization function was needed). Using the UANO-6 basis, correlation of the L shell reduces the IP by 3 cm^{-1} and of the K shell by further 1 cm^{-1} (see Supplemental Material [57]).

In summary, the results for the ionization energy are very promising in terms of obtaining first-principle predictions with an accuracy definitely better than 1 kJ/mol (84 cm^{-1}).

B. Rb_2: The a $^3\Sigma_u^+$ state

Next, we gauge the accuracy of our computational approach for molecular calculations and compute the spectroscopic constants D_e and R_e, i.e., the depth of the interaction potential and its equilibrium distance, for the lowest triplet state $a\,^3\Sigma_u^+$ of Rb_2 . This state plays a fundamental role in photoassociation processes to produce ultracold Rb_2 molecules [33,82–86] and is quite challenging for computational studies due to the shallow nature of the potential, as displayed in Fig. 1. Table II lists the results in a scheme analogous to that used for the IP of atomic Rb.

Interestingly, in comparison to the known experimental reference, the ECP computations deliver the closest result. This close coincidence is largely lucky in view of the estimates for the uncertainty of these values. The uncertainty in the extrapolation is rather small in this case, the results for the CBS limit deviate by less than 0.5 cm^{-1} from the

TABLE II. Computed binding energies D_e and equilibrium bond distances of the $a\,^3\Sigma_u^+$ state of Rb_2. The experimental values are $D_e^{\text{expt}} = 241.5045\ \text{cm}^{-1}$ and $R_e^{\text{expt}} = 6.0650$ Å [87].

	ECP		SFX2C-1e		SFX2C-1e (+M shell)[a]	
	D_e (cm^{-1})	R_e (Å)	D_e (cm^{-1})	R_e (Å)	D_e (cm^{-1})	R_e (Å)
$n = 4$	239.08	6.081	249.20	6.068	249.77	6.058
$n = 5$	241.62	6.069	252.94	6.046	253.90	6.033
$n = 6$	241.90	6.066	253.22	6.044	254.22	6.030
CBS (corr)[b]	242.28	6.062	253.59	6.040	254.64	6.026
CBS (HF+corr)[c]	239.50	6.067	246.31	6.057	247.31	6.044
$+\Delta E_{\text{T}}^{\text{TZ/QZ}}$	237.58	6.067	244.39	6.058	245.39	6.044
$+\Delta E_{\text{(Q)}}^{\text{TZ}} = \text{TBE}$[d]	243.25	6.058	250.09	6.049	251.11	6.036
ΔE_{HLR}			−0.30			

[a] $3s3p3d$ shell included in correlation treatment.
[b] Extrapolation of correlation energy only, Hartree-Fock energy from largest n.
[c] Including a correction for Hartree-Fock limit using the "reference" basis sets.
[d] Theoretical best estimate (see text).

$n = 6$ value in all cases, and the impact on the bond distance is less than 0.005 Å. The effect of core correlation is also very small, the results of the two sets of X2C-1e computations without and with correlation of the M shell differ by only 1 cm^{-1}. A slightly larger correction is imposed by the Hartree-Fock correction, which reduces the binding energy by nearly 3 cm^{-1} for the ECP calculations and 7 cm^{-1} for the all-electron calculations. The high-level corrections for full three-electron clusters and four-electron clusters work in opposite directions, giving corrections of −2 and +6 cm^{-1}, respectively. High-level relativistic corrections turn out to have very little impact on the binding energy, they reduce the binding energy by 0.30 cm^{-1} and thus do not close the small gap between the ECP and the all-electron results. In view of the smallness of this correction (a similar size of correction will be found for Rb_2^+) we decided to not include this value in the total sum for the best estimate but only as indicator for the size of effects due to the approximate treatment of relativistic effects. The total estimate of the uncertainty of the binding energy, obtained in the same way as before for the IP, adds up to ±12 cm^{-1} and thus also spans the difference between the ECP and all-electron calculations. The experimental value lies quite at the border of this range, indicating that the all-electron calculations may have the general tendency of overbinding due to basis-set superposition errors. The predicted equilibrium bond distance follows the trend for the binding energies: The larger the binding energy, the shorter the bond. Again in comparison to the experimental value, the all-electron results give slightly too short bond distances.

For comparison, we performed ECP-based CCSD(T) calculations using the aug-cc-pCVnZ-PP basis sets yielding $(D_e, R_e) = (266.9\ \text{cm}^{-1}, 6.09\ \text{Å})$, $(255.5\ \text{cm}^{-1}, 6.06\ \text{Å})$, and $(245.5\ \text{cm}^{-1}, 6.07\ \text{Å})$ for the $n = 3, 4, 5$ cardinalities, respectively. These computations converge to comparable results, but clearly with a much larger uncertainty for the extrapolation to the CBS limit.

We also assessed the size of the spin-orbit splitting of the triplet state by performing frozen-core MRCI/ECP28MDF/UET17 ($n = 3$) calculations [88–90] using the ECP-LS technique for the corresponding small-core ECP. The computations included seven singlet and seven triplet states of Rb_2, such that in total a 28×28 spin-orbit matrix is set up and diagonalized. The resulting zero-field splittings and energy shifts for the $a\,^3\Sigma_u^+$ state are both $\ll 1\ \text{cm}^{-1}$, which suggests that spin-orbit effects can be neglected in the further discussion. A very small zero-field splitting could also be observed in the X2CAMF computations. This is in accordance with the results reported in Ref. [91] for the $a\,^3\Sigma_u^+$ state of Rb_2, yielding effects in the order of 0.5 cm^{-1} for D_e when comparing numbers obtained with and without SO effects included.

The ROHF-UCCSD(T)/ECP28MDF/UET17 approach was also used to compute a larger set of points of the potential energy curve and the one-dimensional RP-RKHS interpolation method as described in Refs. [92–98] was used to obtain an analytic representation. The respective long-range coefficients required by this procedure were taken from Ref. [85], with $C_6 = 0.227\,003 \times 10^8\ \text{cm}^{-1}\,\text{Å}^6$, $C_8 = 0.778\,289 \times 10^9\ \text{cm}^{-1}\,\text{Å}^8$, and $C_{10} = 0.286\,887 \times 10^{11}\ \text{cm}^{-1}\,\text{Å}^{10}$; cf. Sec. IV B for details on the asymptotic form of interaction potentials. This long-range behavior with three reciprocal power terms defines the RP-RKHS parameters, yielding $n_{\text{Rb}_2} = 3$, $m_{\text{Rb}_2} = 2$, and $s_{\text{Rb}_2} = 2$ as well as $R_a = 18.0\,a_0$. To further provide a physically meaningful short-range description, we imposed a correction of the form

$$V_{\text{SR}}(R) = \frac{a}{R}\exp(-bR). \tag{5}$$

This only affects the PEC for $R < 4.0$ Å and is introduced to correct for inherent artifacts of the RP-RKHS procedure concerning short-range extrapolation [99]. Thus, it has no impact on D_e and R_e but gets relevant for high-energy scattering states ($E > 15\,000\ \text{cm}^{-1}$).

Inspired by the approach reported in Ref. [98], we further provide an empirically adjusted "optimal" PEC for which we scaled and shifted the CBS *ab initio* data in order to match the experimentally derived values D_e^{expt} and R_e^{expt}, respectively [32]. The resulting PEC can be reproduced using our programs and data available from Ref. [100]. In this work, we used this PEC to compute the rovibrational structure of the $a\,^3\Sigma_u^+$ state of Rb_2 . The resulting 41 vibrational levels

TABLE III. Computed binding energies D_e and equilibrium bond distances of the $X\,^2\Sigma_g^+$ state of Rb_2^+.

	ECP		SFX2C-1e		SFX2C-1e (+M shell)[a]	
	D_e (cm^{-1})	R_e (Å)	D_e (cm^{-1})	R_e (Å)	D_e (cm^{-1})	R_e (Å)
$n=4$	6157.6	4.813	6171.9	4.820	6181.4	4.806
$n=5$	6176.8	4.806	6198.1	4.810	6210.5	4.795
$n=6$	6181.5	4.803	6203.8	4.807	6217.0	4.792
CBS (corr)[b]	6187.7	4.801	6210.2	4.804	6224.5	4.788
CBS (HF+corr)[c]	6180.5	4.804	6189.6	4.810	6203.6	4.795
$+\Delta E_{\mathrm{T}}^{\mathrm{TZ/QZ}}$	6177.4	4.806	6186.5	4.812	6200.5	4.797
$+\Delta E_{(\mathrm{Q})}^{\mathrm{TZ}}$ = TBE[d]	6178.8	4.805	6187.9	4.811	6201.9	4.796
ΔE_{HLR}			−0.4			

[a] $3s3p3d$ shell included in correlation treatment.
[b] Extrapolation of correlation energy only, Hartree-Fock energy from largest n.
[c] Including a correction for Hartree-Fock limit using the "reference" basis sets.
[d] Theoretical best estimate (see text).

for $J=0$ are given in Table S.VIII of the Supplemental Material [57]. We observe excellent agreement with experimentally measured levels.

IV. HIGH-ACCURACY RUBIDIUM ION-ATOM INTERACTION POTENTIALS

The previous discussion on Rb ionization energies and spectroscopic constants of the $a\,^3\Sigma_u^+$ triplet ground state of Rb_2 demonstrates the capability of our computational approach to predict energies and potential energy curves to high accuracy. In the following we investigate the binding energies and the full PECs of the two lowest states of Rb_2^+.

A. Accurate binding energies of Rb_2^+

We start out with a discussion of the binding energy and equilibrium distance of the $X\,^2\Sigma_g^+$ state. As already discussed previously [31], there is in our approach a slight consistency error in the asymptotic region, as the symmetry-adapted mean-field (Hartree-Fock) solution formally dissociates the system into two fragments which are a 50:50 mixture of a cation and a neutral atom. Thus, the computed energies in the asymptote do not coincide with the sum of those of the atom and the cation from individual mean-field computations. The consistency could only be achieved by allowing for symmetry-broken solutions in the asymptote. This problem may be fully avoided by special techniques, e.g., the electron attachment equation-of-motion coupled-cluster (EA-EOM-CC) approach [25–27]. However, going to higher-order correlation methods, the effect diminishes and eventually does not significantly contribute to the overall uncertainty of the final result. At the Hartree-Fock level, using the ECP-based approach, the asymptote lies 40 cm^{-1} above the atomic limit, which diminishes to −4.4 cm^{-1} at the CCSD(T) level (nearly independent of the basis set size). At the CCSDT and CCSDT(Q) level, the error shrinks to +1.5 cm^{-1} and +0.7 cm^{-1}, respectively. In the SFX2C-1e scheme, the same observations are made, differing by only 0.3 cm^{-1} from the values quoted above. We will thus in the following report energies relative to those computed for the separated ion and atom. The main results are summarized in Table III, using the same scheme as discussed before.

The CCSD(T) binding energies at the CBS limit differ by approximately 20 cm^{-1} when evaluated from either the ECP or the SFX2C-1e all-electron approach. When correcting for the Hartree-Fock limit, using again large basis sets in both approaches, the difference shrinks to less than 10 cm^{-1}. Correlating the M shell in the latter approach adds 14 cm^{-1} to the binding energy. The difference between ECP and SFX2C-1e results cannot be attributed to remaining high-level relativistic effects. By comparison of SFX2C-1e and SFDC computations, we can estimate a two-electron picture-change effect on the order of −0.14 cm^{-1} whereas going to the two-component X2CAMF scheme gives a correction of the dissociation energy by −0.26 cm^{-1}, resulting in a total ΔE_{HLR} of −0.4 cm^{-1}. The high-level correlation effects are also rather small. Including full triply connected clusters decreases the binding energy by 3 cm^{-1} and the correction from CCSDT(Q) increases it again by approximately half of this value.

Overall, we may estimate an uncertainty of ±10 cm^{-1} for the Hartree-Fock contribution, ±5 cm^{-1} for the extrapolation of the CCSD(T) CBS limit, and ±5 cm^{-1} for high-level correlation effects. Further uncertainties may be correlation effects from even deeper core shells (should not exceed ±5 cm^{-1}) and further relativistic effects (which are also unlikely to exceed ±5 cm^{-1}). Our best estimate for the dissociation energy of Rb_2^+ in the $X\,^2\Sigma_g^+$ state is thus 6202 ± 30 cm^{-1}.

The predicted equilibrium distance changes by less than 0.02 Å among all calculations, except for those with the smallest basis set (see Table III). Correlation of the M shell leads to a small contraction of the distance by 0.01 Å and our best estimate is thus 4.796(10) Å.

The antisymmetric $(1)\,^2\Sigma_u^+$ state also shows a shallow minimum, which is purely due to induced dipole-charge and dispersion effects. The first conclusion is supported by the fact that the computed Hartree-Fock contribution to the binding energy is around 60 cm^{-1} at the equilibrium distance. The best estimate for the binding energy including correlation effects can be deduced from the numbers in Table IV. In this case there are only little effects from basis-set extrapolation, both for the correlation and the Hartree-Fock contribution.

TABLE IV. Computed binding energies D_e and equilibrium bond distances of the $(1)\,^2\Sigma_u^+$ state of Rb_2^+.

	ECP		SFX2C-1e		SFX2C-1e (+ M shell)[a]	
	D_e (cm^{-1})	R_e (Å)	D_e (cm^{-1})	R_e (Å)	D_e (cm^{-1})	R_e (Å)
$n=4$	82.55	12.206	83.88	12.217	83.88	12.196
$n=5$	82.64	12.202	83.95	12.212	83.95	12.191
$n=6$	82.66	12.200	83.97	12.210	83.97	12.189
CBS (corr)[b]	82.65	12.198	83.96	12.208	83.95	12.187
CBS (HF+corr)[c]	82.51	12.205	82.91	12.216	82.90	12.195
$+\Delta E_{\mathrm{T}}^{\mathrm{TZ/QZ}}$	77.14	12.192	77.53	12.204	77.53	12.182
$+\Delta E_{(\mathrm{Q})}^{\mathrm{TZ}} = \mathrm{TBE}$[d]	80.04	12.173	80.43	12.185	80.43	12.163

[a] $3s3p3d$ shell included in correlation treatment.
[b] Extrapolation of correlation energy only, Hartree-Fock energy from largest n.
[c] Including a correction for Hartree-Fock limit using the "reference" basis sets.
[d] Theoretical best estimate (see text).

Likewise, there is only a small discrepancy of 1 cm^{-1} between ECP-based and SFX2C-1e-based computations and a nearly vanishing effect of core correlation. High-level relativistic effects have not been estimated for this case due to technical problems in converging the orbitals, but based on previous experience they are expected to be miniscule. The largest correction comes from high-level correlation effects, a reduction of the binding energy by nearly 5.5 cm^{-1} from the CCSDT calculations and a slight increase again by 2.9 cm^{-1} from CCSDT(Q). The final best estimate is thus 80 ± 9 cm^{-1} for the binding energy.

The equilibrium distance also shows only very little dependence on the basis-set size and the biggest correction comes from the high-level correlation effects, being a shortening by 0.015 Å. There is also some effect of M-core correlation, which shortens the bond length by 0.02 Å in comparison to the computation that keeps this shell uncorrelated. Overall, we may give a best theoretical estimate for R_e of 12.163(20) Å.

B. General long-range form of X_2^+ interaction potentials

An essential aspect of the recent experimental works [1–6] towards entering the ultracold domain of ion-atom interactions relies on studying scattering events. The scattering properties of such collisions are defined by the long-range form of the respective interaction potentials [7]. For ionic dimers with a single active electron (i.e., e.g., alkali-metal systems such as Rb_2^+) this long-range behavior contains the two contributions [14]

$$V_{\mathrm{LR}}(R) = V_{\mathrm{ind/disp}}(R) \pm V_{\mathrm{exch}}(R), \tag{6}$$

where $V_{\mathrm{ind/disp}}(R)$ describes the leading induction and dispersion interaction, while V_{exch} defines the exchange-interaction term. For interactions between an S-state atom and an S-state ion, the first term of Eq. (6) becomes [7]

$$V_{\mathrm{ind/disp}}(R) = -\frac{C_4^{\mathrm{ind}}}{R^4} - \frac{C_6^{\mathrm{ind}}}{R^6} - \frac{C_6^{\mathrm{disp}}}{R^6} + \cdots. \tag{7}$$

In leading order the interaction is due to the charge q of the ion inducing an electric dipole moment of the atom, which reflects in the corresponding induction coefficient

$$C_4^{\mathrm{ind}} = \tfrac{1}{2} q^2 \alpha_{\mathrm{d}}, \tag{8}$$

with the static electric dipole polarizability α_{d} of the atom. The next higher-order induction term is caused by the interaction between the charge of the ion and the induced electric quadrupole moment of the atom, described by the respective coefficient

$$C_6^{\mathrm{ind}} = \tfrac{1}{2} q^2 \alpha_{\mathrm{q}}, \tag{9}$$

with the static electric quadrupole polarizability α_{q} of the atom. The van der Waals–type dispersion interactions are usually weaker, with the leading-order term of Eq. (7) accounting for dynamic interactions due to instantaneous dipole-induced dipole moments of the ion and the atom arising due to quantum fluctuations. Higher-order terms could be added to Eq. (7), but since reaching the s-wave scattering regime for Rb_2^+ is barely possible at all, truncating after the R^{-6} is usually sufficient.

The second term of Eq. (6) is due to the indistinguishability of the two limiting cases Rb+Rb^+ and vice versa. It is thus defined by the energy splitting between the asymptotically degenerate gerade and ungerade states and determines the cross section for resonant charge transfer [101]. For alkali-metal X_2^+ systems, it generally involves one active electron and if both ion and atom are in an S state, it takes the form, in *atomic units* [14,20],

$$V_{\mathrm{exch}}(R) = \frac{V_{X\,^2\Sigma_g^+}(R) - V_{(1)\,^2\Sigma_u^+}(R)}{2} \tag{10a}$$

$$= \frac{1}{2} A R^{\alpha} e^{-\beta R}\left[1 + \frac{B}{R} + \frac{C}{R^2} + \cdots\right]. \tag{10b}$$

In Ref. [14], the parameters α, β, and B are related by simple expressions to the ionization potential I_{Rb} of the Rb atom:

$$\beta = \sqrt{2 I_{\mathrm{Rb}}}, \quad \nu = \frac{1}{\beta}, \quad \alpha = (2\nu - 1), \quad B = \nu^2\left(1 - \frac{1}{2}\nu\right). \tag{11}$$

The corresponding value for the ionization potential is taken from Refs. [80,81], yielding $I_{\mathrm{Rb}}^{\mathrm{expt}} = 0.153\,506\,55\,E_{\mathrm{h}}$ (original measurement: $I_{\mathrm{Rb}}^{\mathrm{expt}} = 33\,690.81 \pm 0.01$ cm^{-1}). The parameter A is the normalization factor of the asymptotic wave function involved to arrive at Eq. (10b) and is given [20,102]

in terms of the parameters of Eq. (11):

$$A = -\frac{\beta^2(2\beta)^{2\nu}\mathrm{e}^{-\nu}}{\Gamma(\nu+1)\Gamma(\nu)}, \tag{12}$$

where $\Gamma(\cdot)$ denotes the gamma function. The second-order expansion coefficient C of Eq. (10b) may be extracted from fits to *ab initio* results and is taken from Ref. [14] with $C = -19.22$.

The characteristic ion-atom interaction length scale R^* may be derived from Eq. (7), yielding [7] $R^* = \sqrt{2\mu C_4\hbar^{-2}}$, which is in general at least one order of magnitude larger than corresponding neutral atom-atom interactions. The corresponding characteristic energy scale $E^* \propto (2\mu^2 C_4)^{-1}$ is at least two orders of magnitude smaller than the one for neutral atom-atom systems. Due to the small reduced mass of Li_2^+, this explains why it was possible to reach the *s*-wave scattering regime in the experimental run described in Ref. [1]. For the Rb_2^+ system, the characteristic interaction length scale is $R^* \approx 5000\,a_0$, with the respective *s*-wave scattering limit $E^* = k_B \times 79$ nK [2]. This stringent temperature requirement is one of the reasons why reaching the quantum collision regime for Rb_2^+ is considerably more difficult as compared to neutral atom systems or to Li_2^+.

C. Construction procedure

The results from Sec. IV A indicate that overall the ROHF-UCCSD(T) approach based on effective core potentials is already quite accurate. We will thus use it for the overall construction of the $X\,^2\Sigma_g^+$ and $(1)\,^2\Sigma_u^+$ potential energy curves and account for higher-level corrections by an appropriate rescaling.

Concerning the CCSD(T) approach for X_2^+ systems in general, our previous work [31] revealed some limitations, as already indicated at the start of this section. In Ref. [31] we demonstrated that CCSD(T) leads to an unphysical long-range barrier of the respective system, which is related to a symmetry instability of the underlying Hartree-Fock mean-field solution. However, our findings also suggested that using (T) corrections from symmetry-broken calculations for the long-range tail and properly merging these with symmetry-adapted solutions for smaller internuclear distances may be a promising approach to construct well-defined and physically meaningful global PECs for the $X\,^2\Sigma_u^+$ and $(1)\,^2\Sigma_u^+$ states of Rb_2^+. The hybrid ROHF-UCCSD(T) energies for both states are defined as [32]

$$E^{\text{hybrid}}_{\text{CCSD(T)}}(R) = E^{D_{2h}}_{\text{ROHF}}(R) + \Delta E^{D_{2h}}_{\text{CCSD}}(R) + \Delta E^{\text{hybrid}}_{\text{(T)}}(R), \tag{13}$$

with the hybrid (T) correction to model the long-range region given by

$$E^{\text{hybrid}}_{\text{CCSD(T)}}(R) = \begin{cases} \Delta E^{C_{2v}}_{(T)}(R) & \text{for} \quad R > R_m, \\ \left[\Delta E^{D_{2h}}_{(T)}(R) + |\Delta E_s|\right] & \text{for} \quad R \leqslant R_m. \end{cases} \tag{14}$$

The first two terms in Eq. (13) denote the ROHF reference energy and the CCSD correlation energy, respectively. The point-group labels represent the computational point groups and correspond to symmetry-adapted (D_{2h}) and symmetry-broken (C_{2v}) solutions. Equation (14) formally represents the use of (T) corrections from symmetry-broken calculations to model the long-range tail and the proper merging to symmetry-adapted (T) corrections at some merging point R_m in the intermediate region to describe the remaining part of the PEC. At R_m the symmetry-adapted values have to be shifted by the respective constant energy difference $|\Delta E_s|$ to the symmetry-broken solution to obtain continuous curves. This construction procedure is schematically illustrated in Fig. 2.

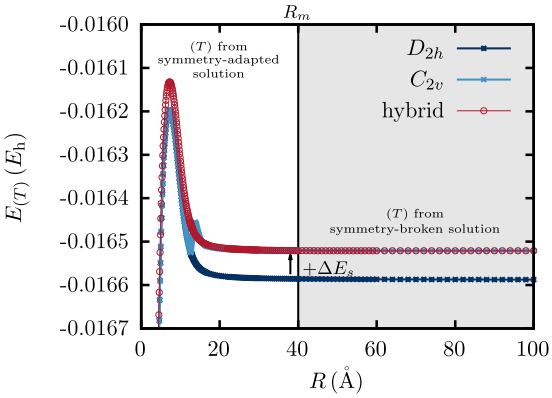

FIG. 2. Schematic visualization of the construction procedure illustrating how to merge symmetry-broken and symmetry-adapted (T) contributions to avoid the repulsive CCSD(T) long-range barrier and to consequently obtain a hybrid ROHF-UCCSD(T) model.

In total energies this shift amounts up to $\approx O(14\ \text{cm}^{-1})$, as can be approximated by the respective differences in Fig. 2. For interaction energies, in particular in the vicinity of the potentials equilibrium $R = 4.8$ Å, the respective difference is in the order of $\approx O(0.5\ \text{cm}^{-1})$. In general, the point R_m [cf. Eq. (14)] enters as an additional free parameter that might be adjusted so to optimally reproduce certain experimental findings (e.g., spectroscopic constants, scattering length, vibrational levels, etc.).

We further note that the small oscillation that occurs in Fig. 2 for the symmetry-broken curve before it collapses to the symmetry-adapted one is a consequence of the numerical bistability of the symmetry-broken CCSD(T) solution in the region where it cannot "decide" whether to collapse to the symmetry-adapted Σ_g or Σ_u state; see Refs. [31,32] for details.

The $X\,^2\Sigma_g^+$ and $(1)\,^2\Sigma_u^+$ states of Rb_2^+ are asymptotically degenerate and thus the construction procedure according to Eqs. (13) and (14) can be applied to obtain physically correct PECs for both states. This implies that in both cases R_m has to be chosen equally, which is only justified if Σ_g and Σ_u are reasonably well degenerate for a given merging parameter R_m. Here, we assume that this is fulfilled if the difference between the total symmetry-adapted ROHF-UCCSD(T) energies is $\leqslant 10^{-8}$ E_h. Moreover, the choice of R_m should be sufficiently far off the repulsive long-range barrier occurring at $R \approx 100$ Å [31]. These two conditions define the restriction

$$27.0\ \text{Å} \leqslant R_m < 50.0\ \text{Å}. \tag{15}$$

We set this value to $R_m = 40.0$ Å for the following discussion.

As shown in the previous section it is important to extrapolate the ROHF-UCCSD(T) results to the respective basis-set

limits. Again, we found an approach based on Eqs. (2) and (3) as the best compromise to obtain the CBS values using the UET17 basis sets. Effects beyond the CCSD(T)/ECP approach, as discussed in Sec. IV A, are now simply included by rescaling the potential energy curves to match D_e and R_e of the theoretical best estimates.

To generate PECs that can be used to study $Rb^+ + Rb$ scattering events, it is inevitable to recover the correct long-range behavior according to Eq. (6). This also involves ensuring that the rescaled *ab initio* data reproduce the theoretically suggested exchange splitting between the gerade and ungerade states as given by Eq. (10b). Details of this correction are given in the Supplemental Material [57]. An overview of exchange splittings $\widetilde{V}_{\text{exch}}$ that result from *ab initio* data and a corresponding comparison with the respective theoretical curve according to Eq. (10b) is given there, as well. Moreover, it is shown that the exchange interaction is very sensitive to the respective basis set leading to an interchange of the Σ_g and Σ_u states, a problem that already occurs at the SCF level.

Finally, the adapted *ab initio* data points [≡ "hybrid ROHF-UCCSD(T)/CBS/mod" level of theory, i.e., those obtained by first transforming according to the hybrid model of Eqs. (13) and (14), followed by a rescaling to the theoretical best estimates for D_e and R_e, and then by subsequent modification to obtain the correct exchange splitting] are passed to the one-dimensional RP-RKHS interpolation method [92–98]. This gives analytical representations for the $X\,^2\Sigma_g^+$ and $(1)\,^2\Sigma_u^+$ PECs and yields by construction the correct leading-order multipole terms according to Eq. (7). It is important to include a sufficient amount of training data in the region $R \in [20.0, 60.0]$ Å to ensure precise interpolation of the exchange interaction [32]. Beyond that region, the training data should be chosen sparsely to ensure extrapolation after Eq. (7). The corresponding induction coefficients follow from the experimentally measured static electric dipole polarizability α_d [103,104] yielding [see Eq. (8)] $C_4^{\text{ind}} = 2.751\,960\,345 \times 10^6$ cm^{-1} Å^4 and from taking the most recent value, based on relativistic coupled-cluster calculations from Ref. [105], for the static electric quadrupole polarizability α_q yielding [see Eq. (9)] $C_6^{\text{ind}} = 0.156\,412\,961 \times 10^8$ cm^{-1} Å^6. The RP-RKHS parameters are chosen as $n_{Rb_2^+} = 2$, $m_{Rb_2^+} = 1$, $s_{Rb_2^+} = 2$, and $R_a = 20.0$ Å for the $X\,^2\Sigma_g^+$ state and $R_a = 85.0$ Å for the $(1)\,^2\Sigma_u^+$ state. Furthermore, Eq. (5) was imposed to provide a physically meaningful short-range description. Again, the RP-RKHS parameters and the short-range correction do not affect D_e and R_e. The resulting PECs can be generated using the PYTHON script and data available from Ref. [106], which are either based on the aug-cc-pCV*n*Z-PP or the UET17 basis-set families both extrapolated to their respective CBS limit. Corresponding data were generated with the hybrid ROHF-UCCSD(T) approach according to Eqs. (13) and (14) and modified to reproduce the correct exchange interaction. This procedure yields the PECs depicted in Fig. 3.

D. Resulting potential energy curves

As displayed in Fig. 3, the ground state of gerade symmetry is much deeper compared to the asymptotically degenerate state of ungerade symmetry, which only shows a rather shallow well at about 12 Å. We note that the choice of the merging

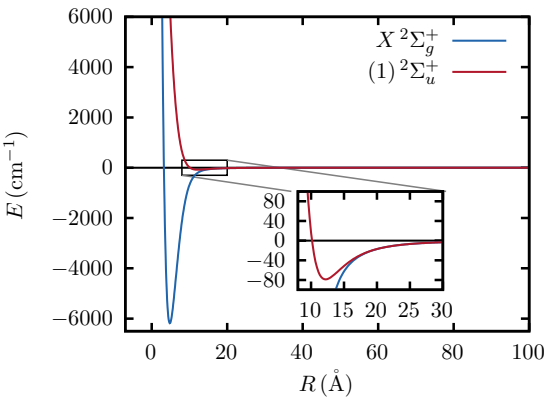

FIG. 3. Potential energy curves of the $X\,^2\Sigma_g^+$ and $(1)\,^2\Sigma_u^+$ states of Rb_2^+ resulting from the RP-RKHS interpolation method based on *ab initio* data obtained at hybrid ROHF-UCCSD(T)/CBS/mod level of theory with the UET17 basis set. The inset shows the shallow potential well corresponding to the ungerade state.

parameter R_m, within the constraints defined by Eq. (15), mainly affects the long-range behavior of the respective PECs. It can thus be viewed as defining a lower bound of the fitting range if the corresponding *ab initio* data were used to extract higher-order induction and dispersion coefficients (i.e., C_6^{disp}, C_8^{ind}, etc.). These higher-order coefficients might improve the quality of the RP-RKHS interpolated PECs by including them into the inherent extrapolation according to Eq. (7). This in turn may be used to screen the sensitivity of subsequent scattering calculations based on these RP-RKHS PECs that account for such higher-order effects. A more detailed discussion on the extraction of induction and dispersion coefficients from hybrid ROHF-UCCSD(T) *ab initio* data may be found in Ref. [32].

As already discussed in Sec. IV C, the choice of the merging point R_m and thus of $|\Delta E_s|$ [cf. Eq. (14)] leaves R_e effectively unchanged and alters D_e by about 0.5 cm^{-1} [32]. The corresponding effects that result from accounting for the theoretically suggested exchange interaction are also very small and give rise to the tiny differences between the theoretical best estimate and the model potential for the binding energies D_e as documented in Table V. The rovibrational ground-state energies, i.e., $(v, J) = (0, 0)$ where v and J denote the vibrational and rotational quantum numbers, were extracted using the LEVEL16 code [107] and the final RP-RKHS potential energy curve. The results are summarized in Table V.

Experimental data given in this table refer to the works already mentioned in the Introduction. The most recent experiment [33] aimed at measuring the ionization potential of $^{85}Rb_2$ formed via photoassociation of ultracold ^{85}Rb atoms (cf. Sec. I). The molecules were subsequently excited by single-photon UV transitions to states above the ionization threshold. This approach yielded an upper limit for the ionization energy of $^{85}Rb_2$ and simultaneously provided a lower bound for D_0 of $^{85}Rb_2^+$, as reported in Table V with $D_0^{\text{expt}} \geqslant 6307.5$ cm^{-1}.

As indicated in Table V, theoretical works on Rb_2^+ found in the literature can be divided into two classes:

TABLE V. Overview of the theoretical best estimates and the binding energies and lowest rovibrational states realized in the fitted model potentials for the $X\,^2\Sigma_g^+$ and $(1)\,^2\Sigma_u^+$ states of Rb_2^+ in comparison to available experiments and other theoretical work.

	$X\,^2\Sigma_g^+$			$(1)\,^2\Sigma_u^+$		
Basis set	D_e (cm^{-1})	D_0 (cm^{-1})	R_e (Å)	D_e (cm^{-1})	D_0 (cm^{-1})	R_e (Å)
TBE	6202 ± 30		4.796 ± 0.010	80.4 ± 9.0		12.163 ± 0.020
Model pot. ($^{87}Rb_2^+$)	6202.02	6179.07	4.796	80.31	78.46	12.163
Model pot. ($^{85}Rb_2^+$)	6202.02	6178.80	4.796	80.31	78.44	12.163
Experiments						
[15,16]	5888 ± 484					
[17]			3.94			
[18]	6049 ± 807					
[33] ($^{85}Rb_2^+$)		$\geqslant 6307.5(6)$				
Theory (model potentials)						
[108]	6936		4.445			
[109]	6977		4.604			
[23]	5816		4.868			
Theory (lcECP+CPP)						
[110]	6130		4.780			
[111]	6365		4.820			
[112] (compact effective potential)	6323		4.731			
[22]	6167		4.794	82		12.1340
[33] ($^{85}Rb_2^+$)		6200 ± 120				

calculations that are based on model potentials [23,108,109] or approaches using large-core effective core potentials (lcECPs) with a core polarization potential (CPP) [22,33,110–112] to account for polarization effects of the core electrons. In the latter approach, spin-orbit effects can be incorporated into the pseudopotential (cf., e.g., Refs. [22,111]). The full valence configuration interaction *ab initio* calculations that accompany the experimental work in Ref. [33] were based on a relativistic nonempirical large-core pseudopotential with CPP. Spin-orbit effects were modeled through a semiempirical spin-orbit pseudopotential and taken into account in the valence CI calculations via the CIPSO procedure (configuration interaction with perturbation including spin-orbit coupling) [91]. As can be inferred from the numbers reported in Ref. [22], the SO effects on the spectroscopic constants of the two lowest states of Rb_2^+ are negligible.

In comparison to the most recent experimental reference value $D_0^{\text{expt}} \geqslant 6307.5$ cm^{-1} (Ref. [33]) the binding energy computed in this work comes out too low by approximately 120 cm^{-1}. While this is in general a satisfactory agreement, the discrepancy is somewhat in conflict with the accuracy estimates given by us previously, which amount to $O(30\ cm^{-1})$.

E. Rovibrational structure

The analysis of the rovibrational term values supported by the $X\,^2\Sigma_g^+$ and $(1)\,^2\Sigma_u^+$ RP-RKHS interpolated PECs based on hybrid ROHF-UCCSD(T)/UET17(CBS)/mod *ab initio* data implies the existence of approximately 280 and 70 vibrational levels ($J = 0$), respectively. These calculations were performed using the LEVEL16 program [107] assuming that Rb_2^+ exclusively contains the ^{85}Rb isotope. From a fit to the lower part of the spectrum (up to $v = 50$ and 20 for the two potentials) to a Dunham expansion, the spectroscopic constants listed in Table VI can be extracted. The corresponding values for $^{87}Rb_2^+$ are listed in the Supplemental Material [57]. The rovibrational structures of the two states for $(v, J = 0)$ are shown in Figs. 4(a) and 4(b). The level spacings of the deeply bound vibrational states of the $X\,^2\Sigma_g^+$ state amount to about 46 cm^{-1}, close to values reported from earlier computations [33].

The $(1)\,^2\Sigma_u^+$ potential is extremely shallow as reflected by $\omega_e \approx 3.8$ cm^{-1}. Despite its well depth of only $\approx$80 cm^{-1} it still can support more vibrational levels than the $a\,^3\Sigma_u$ state of Rb_2 (cf. Table S.V in the Supplemental Material [57]) with a potential depth of $\approx$241 cm^{-1}, for which only 41 bound states are found. This is a direct consequence of the exceedingly large interaction length scale R^* of Rb_2^+, which is at least one order of magnitude larger as compared to the neutral species [7].

TABLE VI. Spectroscopic constants of the $^{85}Rb_2^+$ states obtained by a fit to the lowest rovibrational states ($v \in \{0, 1, \ldots, 50\}$, $J \in \{0, 1, \ldots, 20\}$ for the $X\,^2\Sigma_g^+$ state and $v \in \{0, 1, \ldots, 20\}$, $J \in \{0, 1, \ldots, 10\}$ for the $(1)\,^2\Sigma_u^+$ state).

Parameter	$X\,^2\Sigma_g^+$	$(1)\,^2\Sigma_u^+$
ω_e (cm^{-1})	46.482	3.767
$\omega_e x_e$ (cm^{-1})	8.05×10^{-2}	5.25×10^{-2}
$\omega_e y_e$ (cm^{-1})	9.04×10^{-5}	2.46×10^{-5}
$\omega_e z_e$ (cm^{-1})	-6.19×10^{-7}	3.10×10^{-6}
B_e (cm^{-1})	1.72×10^{-2}	2.61×10^{-3}
D_e (cm^{-1})	-8.94×10^{-8}	-1.94×10^{-6}
H_e (cm^{-1})	-2.90×10^{-10}	-2.15×10^{-8}
L_e (cm^{-1})	$< 1\times10^{-12}$	8.80×10^{-11}
α_e (cm^{-1})	3.96×10^{-5}	3.90×10^{-5}
β_e (cm^{-1})	4.35×10^{-10}	1.08×10^{-8}
γ_e (cm^{-1})	-8.14×10^{-9}	-1.45×10^{-7}

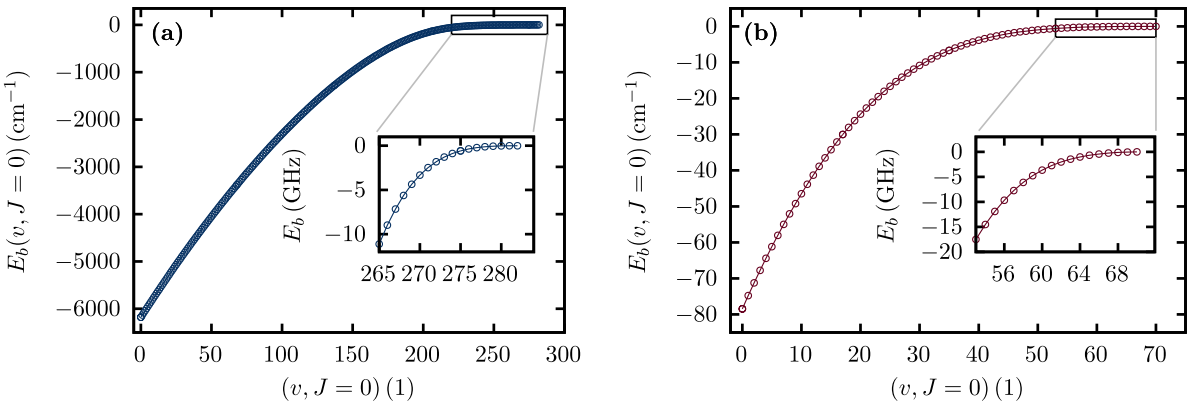

FIG. 4. Computed vibrational levels ($J = 0$) of (a) the $X\,^2\Sigma_g^+$ state and (b) the $(1)\,^2\Sigma_u^+$ state. The results correspond to the Rb_2^+ system which only contains the ^{85}Rb isotope.

All data generated by the LEVEL16 code can be found in the Supplemental Material [57], which also includes the corresponding input files for technical details and to rerun our calculations. An analogous study based on the aug-cc-pCVnZ-PP basis-set series and referring to Rb_2^+ containing merely the ^{87}Rb isotope may be found in Ref. [32].

V. CONCLUSIONS

This work provides a protocol for computing highly accurate binding energies and accurate global PECs for the ground state of Rb_2^+ within an additivity scheme based on ROHF-UCCSD(T) calculations. The approach circumvents our recently revealed limitations of perturbative coupled-cluster approximations by using a hybrid model with symmetry-broken (T) corrections describing the respective long-range part of the PEC properly merged to symmetry-adapted solutions for smaller internuclear distances. Furthermore, the construction procedure is designed such that the PECs for the $X\,^2\Sigma_g^+$ and $(1)\,^2\Sigma_u^+$ states of Rb_2^+ reproduce the physically correct exchange splitting. This is particularly important when using the corresponding potentials for highly accurate studies in the context of ultracold chemistry, e.g., for scattering calculations. In this regard, we moreover provide ready-to-use analytical PEC representations obtained within the framework of RP-RKHS interpolation.

We benchmarked the accuracy of our computational method for ionization energies of Rb as well as for spectroscopic constants and vibrational levels of the $a\,^3\Sigma_u^+$ triplet ground state of Rb_2. In both cases we obtained very good agreement with respective experimental findings, which confirms the tight error bars estimated for the uncertainty of the computed values. While in this respect including high-level correlation (HLC) contributions and high-level relativistic corrections are essential for ionization energies, we found that they are of much less importance for interaction energies. For both Rb_2 and Rb_2^+, HLC effects are in the order of ≈2–3 cm^{-1} for the total binding energy.

Our computational approach gives a value of 6202 ± 30 cm^{-1} for the dissociation energy of the $X\,^2\Sigma_g^+$ state and 80.4 ± 9.0 cm^{-1} for the antibonding $(1)\,^2\Sigma_u^+$ state. We also investigated the rovibrational structure of these states based on the model potentials fitted to our computed values using the RP-RKHS approach. In particular we get a lowest rovibrational state in the $X\,^2\Sigma_g^+$ with a binding energy of 6179 cm^{-1}. There is a residual deviation of approximately 130 cm^{-1} from the most recent experimental estimate for the lower bound on the binding energy of Rb_2^+. This is a closer agreement as compared to other theoretical works on X_2^+ systems, with $X \in \{\text{Li, Na, K, Rb}\}$. However, the discrepancy is significantly larger than the estimate for the residual uncertainty of our computations. This will certainly require further theoretical and experimental investigations.

The data that support the findings of this study are available within the article and its Supplemental Material [57].

ACKNOWLEDGMENTS

J.S. and A.K. acknowledge funding by IQST. The research of IQST is financially supported by the Ministry of Science, Research, and Arts Baden-Württemberg. The authors furthermore acknowledge support by the state of Baden-Württemberg through bwHPC and the German Research Foundation (DFG) through Grant No. INST 40/575-1 FUGG (JUSTUS 2 cluster). The work at Johns Hopkins University was supported by the National Science Foundation under Grant No. PHY-2011794.

[1] T. Schmid, C. Veit, N. Zuber, R. Löw, T. Pfau, M. Tarana, and M. Tomza, Phys. Rev. Lett. **120**, 153401 (2018).

[2] K. S. Kleinbach, F. Engel, T. Dieterle, R. Löw, T. Pfau, and F. Meinert, Phys. Rev. Lett. **120**, 193401 (2018).

[3] F. Engel, T. Dieterle, T. Schmid, C. Tomschitz, C. Veit, N. Zuber, R. Löw, T. Pfau, and F. Meinert, Phys. Rev. Lett. **121**, 193401 (2018).

[4] T. Dieterle, M. Berngruber, C. Hölzl, R. Löw, K. Jachymski, T. Pfau, and F. Meinert, Phys. Rev. A **102**, 041301(R) (2020).

[5] T. Dieterle, M. Berngruber, C. Hölzl, R. Löw, K. Jachymski, T. Pfau, and F. Meinert, Phys. Rev. Lett. **126**, 033401 (2021).

[6] C. Veit, N. Zuber, O. A. Herrera-Sancho, V. S. V. Anasuri, T. Schmid, F. Meinert, R. Löw, and T. Pfau, Phys. Rev. X **11**, 011036 (2021).

[7] M. Tomza, K. Jachymski, R. Gerritsma, A. Negretti, T. Calarco, Z. Idziaszek, and P. S. Julienne, Rev. Mod. Phys. **91**, 035001 (2019).

[8] R. Côté and A. Dalgarno, Phys. Rev. A **62**, 012709 (2000).

[9] Z. Idziaszek, T. Calarco, P. S. Julienne, and A. Simoni, Phys. Rev. A **79**, 010702(R) (2009).

[10] K. Jachymski, M. Krych, P. S. Julienne, and Z. Idziaszek, Phys. Rev. Lett. **110**, 213202 (2013).

[11] W. Casteels, J. Tempere, and J. T. Devreese, J. Low Temp. Phys. **162**, 266 (2011).

[12] G. E. Astrakharchik, L. A. P. n. Ardila, R. Schmidt, K. Jachymski, and A. Negretti, Commun. Phys. **4**, 94 (2021).

[13] U. Bissbort, D. Cocks, A. Negretti, Z. Idziaszek, T. Calarco, F. Schmidt-Kaler, W. Hofstetter, and R. Gerritsma, Phys. Rev. Lett. **111**, 080501 (2013).

[14] R. Côté, in *Advances In Atomic, Molecular, and Optical Physics*, Vol. 65, edited by E. Arimondo, C. C. Lin, and S. F. Yelin (Academic, New York, 2016), pp. 67–126

[15] Y. Lee and B. H. Mahan, J. Chem. Phys. **42**, 2893 (1965).

[16] M. Shafi, C. L. Beckel, and R. Engelke, J. Mol. Spectrosc. **42**, 578 (1972).

[17] R. E. Olson, Phys. Rev. **187**, 153 (1969).

[18] G. S. Wagner and N. R. Isenor, Can. J. Phys. **63**, 976 (1985).

[19] K. Jachymski and F. Meinert, Appl. Sci. **10**, 2371 (2020).

[20] S. Magnier, S. Rousseau, A. Allouche, G. Hadinger, and M. Aubert-Frécon, Chem. Phys. **246**, 57 (1999).

[21] S. Magnier and M. Aubert-Frécon, J. Quant. Spectrosc. Radiat. Transfer **78**, 217 (2003).

[22] A. Jraij, A. Allouche, M. Korek, and M. Aubert-Frécon, Chem. Phys. **290**, 129 (2003).

[23] M. Aymar, S. Azizi, and O. Dulieu, J. Phys. B: At., Mol. Opt. Phys. **36**, 4799 (2003).

[24] H. Berriche, Int. J. Quantum Chem. **113**, 2405 (2013).

[25] M. Musiał, M. Medrek, and S. A. Kucharski, Mol. Phys. **113**, 2943 (2015).

[26] A. Bewicz, M. Musiał, and S. A. Kucharski, Mol. Phys. **115**, 2649 (2017).

[27] P. Skupin, M. Musiał, and S. A. Kucharski, J. Phys. Chem. A **121**, 1480 (2017).

[28] A. Tajti, P. G. Szalay, A. G. Császár, M. Kállay, J. Gauss, E. F. Valeev, B. A. Flowers, J. Vázquez, and J. F. Stanton, J. Chem. Phys. **121**, 11599 (2004).

[29] Y. J. Bomble, J. Vázquez, M. Kállay, C. Michauk, P. G. Szalay, A. G. Császár, J. Gauss, and J. F. Stanton, J. Chem. Phys. **125**, 064108 (2006).

[30] M. E. Harding, J. Vázquez, B. Ruscic, A. K. Wilson, J. Gauss, and J. F. Stanton, J. Chem. Phys. **128**, 114111 (2008).

[31] J. Schnabel, L. Cheng, and A. Köhn, J. Chem. Phys. **155**, 124101 (2021).

[32] J. Schnabel, Theoretical investigations for photoassociation and ion-atom scattering experiments in ultracold rubidium gases, Ph.D. thesis, University of Stuttgart, 2021, https://dx.doi.org/10.18419/opus-11852

[33] M. A. Bellos, R. Carollo, J. Banerjee, M. Ascoli, A.-R. Allouche, E. E. Eyler, P. L. Gould, and W. C. Stwalley, Phys. Rev. A **87**, 012508 (2013).

[34] K. Jachymski, M. Krych, P. S. Julienne, and Z. Idziaszek, Phys. Rev. A **90**, 042705 (2014).

[35] D. Feller, J. Chem. Phys. **98**, 7059 (1993).

[36] T. Helgaker, W. Klopper, H. Koch, and J. Noga, J. Chem. Phys. **106**, 9639 (1997).

[37] J. M. L. Martin and G. de Oliveira, J. Chem. Phys. **111**, 1843 (1999).

[38] M. S. Schuurman, S. R. Muir, W. D. Allen, and H. F. Schaefer III, J. Chem. Phys. **120**, 11586 (2004).

[39] D. Feller, K. A. Peterson, and D. A. Dixon, J. Chem. Phys. **129**, 204105 (2008).

[40] I. S. Lim, P. Schwerdtfeger, B. Metz, and H. Stoll, J. Chem. Phys. **122**, 104103 (2005).

[41] K. G. Dyall, J. Chem. Phys. **115**, 9136 (2001).

[42] W. Liu and D. Peng, J. Chem. Phys. **131**, 031104 (2009).

[43] K. Raghavachari, G. W. Trucks, J. A. Pople, and M. Head-Gordon, Chem. Phys. Lett. **157**, 479 (1989).

[44] R. J. Bartlett, J. D. Watts, S. A. Kucharski, and J. Noga, Chem. Phys. Lett. **165**, 513 (1990).

[45] C. Hampel, K. A. Peterson, and H.-J. Werner, Chem. Phys. Lett. **190**, 1 (1992).

[46] J. D. Watts, J. Gauss, and R. J. Bartlett, Chem. Phys. Lett. **200**, 1 (1992).

[47] J. Noga and R. J. Bartlett, J. Chem. Phys. **86**, 7041 (1987).

[48] J. Noga and R. J. Bartlett, J. Chem. Phys. **89**, 3401 (1988).

[49] G. E. Scuseria and H. F. Schaefer III, Chem. Phys. Lett. **152**, 382 (1988).

[50] J. D. Watts and R. J. Bartlett, J. Chem. Phys. **93**, 6104 (1990).

[51] S. A. Kucharski and R. J. Bartlett, Chem. Phys. Lett. **158**, 550 (1989).

[52] Y. J. Bomble, J. F. Stanton, M. Kállay, and J. Gauss, J. Chem. Phys. **123**, 054101 (2005).

[53] M. Kállay and J. Gauss, J. Chem. Phys. **123**, 214105 (2005).

[54] M. Kállay and J. Gauss, J. Chem. Phys. **129**, 144101 (2008).

[55] J. G. Hill and K. A. Peterson, J. Chem. Phys. **147**, 244106 (2017).

[56] J. Schnabel, T. Kampschulte, S. Rupp, J. Hecker Denschlag, and A. Köhn, Phys. Rev. A **103**, 022820 (2021).

[57] See Supplemental Material at http://link.aps.org/supplemental/10.1103/PhysRevA.106.032804 for details on technical aspects, which includes in addition Refs. [113–115], and for further tables, figures, as well as for all data that support the findings of this study.

[58] B. O. Roos, V. Veryazov, and P.-O. Widmark, Theor. Chem. Acc. **111**, 345 (2004).

[59] A. Halkier, T. Helgaker, P. Jørgensen, W. Klopper, H. Koch, J. Olsen, and A. K. Wilson, Chem. Phys. Lett. **286**, 243 (1998).

[60] J. M. Martin, Chem. Phys. Lett. **259**, 669 (1996).

[61] D. Feller, K. A. Peterson, and J. G. Hill, J. Chem. Phys. **135**, 044102 (2011).

[62] D. Feller, J. Chem. Phys. **138**, 074103 (2013).

[63] M. Lesiuk and B. Jeziorski, J. Chem. Theory Comput. **15**, 5398 (2019).

[64] P. Pyykkö, Chem. Rev. **112**, 371 (2012).

[65] P. Schwerdtfeger, O. R. Smits, and P. Pyykkö, Nat. Rev. Chem. **4**, 359 (2020).

[66] K. Kozioł and G. A. Aucar, J. Chem. Phys. **148**, 134101 (2018).

[67] K. G. Dyall, J. Chem. Phys. **100**, 2118 (1994).

[68] J. Liu and L. Cheng, J. Chem. Phys. **148**, 144108 (2018).

[69] C. Zhang and L. Cheng, J. Chem. Phys. A **126**, 4537 (2022).

[70] H.-J. Werner, P. J. Knowles, G. Knizia, F. R. Manby, and M. Schütz, WIREs Comput. Mol. Sci. **2**, 242 (2012).

[71] H.-J. Werner, P. J. Knowles, F. R. Manby, J. A. Black, K. Doll, A. Heßelmann, D. Kats, A. Köhn, T. Korona, D. A. Kreplin, Q. Ma, T. F. Miller, A. Mitrushchenkov, K. A. Peterson, I. Polyak, G. Rauhut, and M. Sibaev, J. Chem. Phys. **152**, 144107 (2020).

[72] H.-J. Werner, P. J. Knowles, G. Knizia, F. R. Manby, M. Schütz *et al.*, Molpro, version 2019.2, a package of ab initio programs, see http://www.molpro.net.

[73] J. F. Stanton, J. Gauss, L. Cheng, M. E. Harding, D. A. Matthews, and P. G. Szalay, CFOUR, Coupled-Cluster techniques for Computational Chemistry, a quantum-chemical program package, with contributions from A.A. Auer, R.J. Bartlett, U. Benedikt, C. Berger, D.E. Bernholdt, S. Blaschke, Y. J. Bomble, S. Burger, O. Christiansen, D. Datta *et al.*, and the integral packages MOLECULE (J. Almlöf and P.R. Taylor), PROPS (P.R. Taylor), ABACUS (T. Helgaker, H.J. Aa. Jensen, P. Jørgensen, and J. Olsen), and ECP routines by A. V. Mitin and C. van Wüllen. For the current version, see http://www.cfour.de.

[74] D. A. Matthews, L. Cheng, M. E. Harding, F. Lipparini, S. Stopkowicz, T.-C. Jagau, P. G. Szalay, J. Gauss, and J. F. Stanton, J. Chem. Phys. **152**, 214108 (2020).

[75] L. Cheng and J. Gauss, J. Chem. Phys. **135**, 084114 (2011).

[76] J. Liu, Y. Shen, A. Asthana, and L. Cheng, J. Chem. Phys. **148**, 034106 (2018).

[77] M. Kállay, P. R. Nagy, Z. Rolik, D. Mester, G. S. J. Csontos, J. Csóka, B. P. Szabó, L. Gyevi-Nagy, I. Ladjánszki, L. Szegedy, B. Ladóczki, K. Petrov, M. Farkas, P. D. Mezei, and B. Hégely, MRCC, a quantum chemical program suite, 2019, see www.mrcc.hu.

[78] M. Kállay and P. R. Surján, J. Chem. Phys. **115**, 2945 (2001).

[79] M. Kállay, P. R. Nagy, D. Mester, Z. Rolik, G. Samu, J. Csontos, J. Csóka, P. B. Szabó, L. Gyevi-Nagy, B. Hégely, I. Ladjánszki, L. Szegedy, B. Ladóczki, K. Petrov, M. Farkas, P. D. Mezei, and A. Ganyecz, J. Chem. Phys. **152**, 074107 (2020).

[80] A. Kramida, Y. Ralchenko, J. Reader, and and NIST ASD Team, NIST Atomic Spectra Database (ver. 5.6.1), https://physics.nist.gov/asd.

[81] C.-J. Lorenzen and K. Niemax, Phys. Scr. **27**, 300 (1983).

[82] W. C. Stwalley and H. Wang, J. Mol. Spectrosc. **195**, 194 (1999).

[83] K. M. Jones, E. Tiesinga, P. D. Lett, and P. S. Julienne, Rev. Mod. Phys. **78**, 483 (2006).

[84] J. Ulmanis, J. Deiglmayr, M. Repp, R. Wester, and M. Weidemüller, Chem. Rev. **112**, 4890 (2012).

[85] C. Strauss, T. Takekoshi, F. Lang, K. Winkler, R. Grimm, J. Hecker Denschlag, and E. Tiemann, Phys. Rev. A **82**, 052514 (2010).

[86] M. A. Bellos, D. Rahmlow, R. Carollo, J. Banerjee, O. Dulieu, A. Gerdes, E. E. Eyler, P. L. Gould, and W. C. Stwalley, Phys. Chem. Chem. Phys. **13**, 18880 (2011).

[87] Y. Guan, X. Han, J. Yang, Z. Zhou, X. Dai, E. H. Ahmed, A. M. Lyyra, S. Magnier, V. S. Ivanov, A. S. Skublov, and V. B. Sovkov, J. Chem. Phys. **139**, 144303 (2013).

[88] H.-J. Werner and P. J. Knowles, J. Chem. Phys. **89**, 5803 (1988).

[89] P. J. Knowles and H.-J. Werner, Chem. Phys. Lett. **145**, 514 (1988).

[90] P. J. Knowles and H.-J. Werner, Theor. Chim. Acta **84**, 95 (1992).

[91] A.-R. Allouche and M. Aubert-Frécon, J. Chem. Phys. **136**, 114302 (2012).

[92] T. Ho and H. Rabitz, J. Chem. Phys. **104**, 2584 (1996).

[93] T. Hollebeek, T.-S. Ho, and H. Rabitz, Annu. Rev. Phys. Chem. **50**, 537 (1999).

[94] T.-S. Ho, H. Rabitz, and G. Scoles, J. Chem. Phys. **112**, 6218 (2000).

[95] T.-S. Ho and H. Rabitz, J. Chem. Phys. **113**, 3960 (2000).

[96] J. Higgins, T. Hollebeek, J. Reho, T.-S. Ho, K. K. Lehmann, H. Rabitz, G. Scoles, and M. Gutowski, J. Chem. Phys. **112**, 5751 (2000).

[97] O. T. Unke and M. Meuwly, J. Chem. Inf. Model. **57**, 1923 (2017).

[98] P. Soldán, J. Chem. Phys. **132**, 234308 (2010).

[99] P. Soldán and J. M. Hutson, J. Chem. Phys. **112**, 4415 (2000).

[100] J. Schnabel and A. Köhn, RP-RKHS-based interpolation to generate rubidium dimer and trimer potential energy surfaces, see https://doi.org/10.5281/zenodo.5379475.

[101] J. N. Bardsley, T. Holstein, B. R. Junker, and S. Sinha, Phys. Rev. A **11**, 1911 (1975).

[102] B. M. Smirnov, Phys. Usp. **44**, 221 (2001).

[103] P. Schwerdtfeger and J. K. Nagle, Mol. Phys. **117**, 1200 (2019).

[104] M. D. Gregoire, I. Hromada, W. F. Holmgren, R. Trubko, and A. D. Cronin, Phys. Rev. A **92**, 052513 (2015).

[105] J. Kaur, D. K. Nandy, B. Arora, and B. K. Sahoo, Phys. Rev. A **91**, 012705 (2015).

[106] J. Schnabel and A. Köhn, A RP-RKHS-based ion-atom interaction potential generator for the rubidium dimer cation, see https://doi.org/10.5281/zenodo.5994230.

[107] R. J. L. Roy, J. Quant. Spectrosc. Radiat. Transfer **186**, 167 (2017).

[108] L. Bellomonte, P. Cavaliere, and G. Ferrante, J. Chem. Phys. **61**, 3225 (1974).

[109] S. H. Patil and K. T. Tang, J. Chem. Phys. **113**, 676 (2000).

[110] L. von Szentpály, P. Fuentealba, H. Preuss, and H. Stoll, Chem. Phys. Lett. **93**, 555 (1982).

[111] H. Silberbach, P. Schwerdtfeger, H. Stoll, and H. Preuss, J. Phys. B: At. Mol. Phys. **19**, 501 (1986).

[112] M. Krauss and W. J. Stevens, J. Chem. Phys. **93**, 4236 (1990).

[113] D. P. Tew and W. Klopper, J. Chem. Phys. **125**, 094302 (2006).

[114] S. Huzinaga and B. Miguel, Chem. Phys. Lett. **175**, 289 (1990).

[115] S. Huzinaga and M. Klobukowski, Chem. Phys. Lett. **212**, 260 (1993).